

Document downloaded from:

<http://hdl.handle.net/10251/45556>

This paper must be cited as:

Adrián Martínez, S.; Ageron, M.; Aguilar, JA.; Aharonian, F.; Aiello, S.; Albert, A.; Alexandri, M.... (2013). Expansion cone for the 3-inch PMTs of the KM3NeT optical modules. *Journal of Instrumentation*. 8(3):1-19. doi:10.1088/1748-0221/8/03/T03006.



The final publication is available at

<http://dx.doi.org/10.1088/1748-0221/8/03/T03006>

Copyright IOP Publishing: Hybrid Open Access

Additional Information

Document downloaded from:

<http://hdl.handle.net/10251/45556>

This paper must be cited as:

Adrián Martínez, S.; Ardid Ramírez, M.; Bou Cabo, M.; Espinosa Roselló, V.; Ferri García, M.; Llorens Alvarez, CD.; Lloret, J.... (2013). Expansion cone for the 3-inch PMTs of the KM3NeT optical modules. *Journal of Instrumentation*. 8(3):1-19. doi:10.1088/1748-0221/8/03/T03006.



The final publication is available at

<http://dx.doi.org/10.1088/1748-0221/8/03/T03006>

Copyright IOP Publishing: Hybrid Open Access

Expansion cone for the 3-inch PMTs of the KM3NeT Optical Modules

The KM3NeT Collaboration

*S. Adrián-Martínez*⁴⁵, *M. Ageron*⁹, *J.A. Aguilar*¹⁶, *F. Aharonian*¹¹, *S. Aiello*²¹, *A. Albert*¹³,
*M. Alexandri*¹⁴, *F. Ameli*²⁹, *E.G. Anassontzis*⁴, *M. Anghinolfi*²³, *G. Anton*¹², *S. Anvar*⁶,
*M. Ardid*⁴⁵, *A. Assis Jesus*³⁹, *J.-J. Aubert*⁹, *R. Bakker*⁴⁰, *A.E. Ball*⁴¹, *G. Barbarino*²⁷,
*E. Barbarito*¹⁸, *F. Barbato*²⁷, *B. Baret*³, *M. de Bel*², *A. Belias*^{41,14}, *N. Bellou*³⁴, *E. Berbee*³⁹,
*A. Berkien*³⁹, *A. Bersani*²³, *V. Bertin*⁹, *S. Beurthey*⁹, *S. Biagi*¹⁹, *C. Bigongiari*¹⁶, *B. Bigourdan*¹⁷,
*M. Billault*⁹, *R. de Boer*³⁹, *H. Boer Rookhuizen*³⁹, *M. Bonori*³⁰, *M. Borghini*⁸, *M. Bou-Cabo*⁴⁵,
*B. Bouhadef*²⁸, *G. Bourlis*¹⁵, *M. Bouwhuis*³⁹, *S. Bradbury*³⁶, *A. Brown*⁹, *F. Bruni*⁴³, *J. Brunner*⁹,
*M. Brunoldi*²³, *J. Busto*⁹, *G. Cacopardo*²⁴, *L. Caillaud*⁹, *D. Calvo Díaz-Aldagalán*¹⁶, *A. Calzas*⁹,
*M. Canals*⁵, *A. Capone*³⁰, *J. Carr*⁹, *E. Castorina*²⁸, *S. Cecchini*¹⁹, *A. Ceres*¹⁸, *R. Cereseto*²³,
*Th. Chaleil*⁶, *F. Chateau*⁶, *T. Chiarusi*¹⁹, *D. Choqueuse*¹⁷, *P.E. Christopoulou*¹⁵, *G. Chronis*¹⁴,
*O. Ciaffoni*²⁵, *M. Circella*¹⁸, *R. Cocimano*²⁴, *F. Cohen*¹³, *F. Colijn*³⁴, *R. Coniglione*²⁴,
*M. Cordelli*²⁵, *A. Cosquer*⁹, *M. Costa*²⁴, *P. Coyle*⁹, *J. Craig*¹, *A. Creusot*³, *C. Curti*⁹,
*A. D'Amico*²⁴, *G. Damy*¹⁷, *R. De Asmundis*²⁶, *G. De Bonis*³⁰, *G. Decock*⁶, *P. Decowski*³⁹,
*E. Delagnes*⁶, *G. De Rosa*²⁷, *C. Distefano*²⁴, *C. Donzaud*^{3,a}, *D. Dornic*⁹,
*Q. Dorosti-Hasankiadeh*³⁵, *J. Drogou*¹⁷, *D. Drouhin*¹³, *F. Druillolle*⁶, *L. Drury*¹¹, *D. Durand*⁶,
*G.A. Durand*⁶, *T. Eberl*¹², *U. Emanuele*¹⁶, *A. Enzenhöfer*¹², *J.-P. Ernenwein*⁹, *S. Escoffier*⁹,
*V. Espinosa*⁴⁵, *G. Etiopie*³¹, *P. Favali*³¹, *D. Felea*³³, *M. Ferri*⁴⁵, *S. Ferry*⁶, *V. Flaminio*²⁸,
*F. Folger*¹², *A. Fotiou*⁴¹, *U. Fritsch*¹², *D. Gajanana*³⁹, *R. Garaguso*²⁸, *G.P. Gasparini*⁸,
*F. Gasparoni*⁴³, *V. Gautard*⁶, *F. Gensolen*⁹, *K. Geyer*¹², *G. Giacomelli*¹⁹, *I. Gialas*¹⁵,
*V. Giordano*²⁴, *J. Giraud*⁶, *N. Gizani*¹⁵, *A. Gleixner*¹², *C. Gojak*⁹, *J.P. Gómez-González*¹⁶,
*K. Graf*¹², *D. Grasso*²⁸, *A. Grimaldi*²¹, *R. Groenewegen*⁴⁰, *Z. Guédé*¹⁷, *G. Guillard*³²,
*F. Guilloux*⁶, *R. Habel*²⁵, *G. Hallewell*⁹, *H. van Haren*⁴⁰, *J. van Heerwaarden*⁴⁰, *A. Heijboer*³⁹,
*E. Heine*³⁹, *J.J. Hernández-Rey*¹⁶, *B. Herold*¹², *M. van de Hoek*³⁹, *J. Hogenbirk*³⁹, *J. Hößl*¹²,
*C.C. Hsu*³⁹, *M. Imbessi*²⁴, *A. Jamieson*¹, *P. Jansweijer*³⁹, *M. de Jong*³⁹, *F. Jouvenot*³⁷,
M. Kadler^{12,b}, *N. Kalantar-Nayestanaki*³⁵, *O. Kalekin*¹², *A. Kappes*^{12,c}, *M. Karolak*⁶,
*U.F. Katz*¹², *O. Kavatsyuk*^{35*}, *P. Keller*⁹, *Y. Kiskiras*⁴¹, *R. Klein*¹², *H. Kok*³⁹, *H. Kontoyiannis*¹⁴,
P. Kooijman^{2,39,44}, *J. Koopstra*^{2,39}, *C. Kopper*^{39,d}, *A. Korporaal*³⁹, *P. Koske*³⁴, *A. Kouchner*³,
*S. Koutsoukos*⁴, *I. Kreykenbohm*¹², *V. Kulikovskiy*^{23,e}, *M. Laan*⁴⁰, *C. La Fratta*³¹, *P. Lagier*⁹,
*R. Lahmann*¹², *P. Lamare*⁹, *G. Larosa*⁴⁵, *D. Lattuada*²⁴, *A. Leisos*¹⁵, *D. Lenis*¹⁵, *E. Leonora*²¹,
*H. Le Provost*⁶, *G. Lim*², *C.D. Llorens*⁴⁵, *J. Lloret*⁴⁵, *H. Löhner*^{35,†}, *D. Lo Presti*²², *P. Lotrus*⁶,
*F. Louis*⁶, *F. Lucarelli*³⁰, *V. Lykousis*¹⁴, *D. Malyshev*^{11,f}, *S. Mangano*¹⁶, *E.C. Marcoulaki*³⁸,
*A. Margiotta*¹⁹, *G. Marinaro*³¹, *A. Marinelli*²⁸, *O. Mariş*³³, *E. Markopoulos*⁴¹, *C. Markou*³⁸,
*J.A. Martínez-Mora*⁴⁵, *A. Martini*²⁵, *J. Marvaldi*¹⁷, *R. Masullo*³⁰, *G. Maurin*^{6,g}, *P. Migliozi*²⁶,
*E. Migneco*²⁴, *S. Minutoli*²³, *A. Miraglia*²⁴, *C.M. Mollo*²⁶, *M. Mongelli*¹⁸, *E. Monmarthe*⁶,
*M. Morganti*²⁸, *S. Mos*³⁹, *H. Motz*^{12,h}, *Y. Moudén*⁶, *G. Mul*³⁹, *P. Musico*²³, *M. Musumeci*²⁴,
Ch. Naumann^{6,i}, *M. Neff*¹², *C. Nicolaou*¹⁰, *A. Orlando*²⁴, *D. Palioselitis*³⁹, *K. Papageorgiou*¹⁵,
*A. Papaikonomou*⁴, *R. Papaleo*²⁴, *I.A. Papazoglou*³⁸, *G.E. Pāvālas*³³, *H.Z. Peek*³⁹, *J. Perkin*⁴²,
*P. Piattelli*²⁴, *V. Popa*³³, *T. Pradier*³², *E. Presani*³⁹, *I.G. Friede*¹, *A. Psallidas*⁴¹, *C. Rabouille*⁷,
*C. Racca*¹³, *A. Radu*³³, *N. Randazzo*²¹, *P.A. Rapidis*³⁸, *P. Razis*¹⁰, *D. Real*¹⁶, *C. Reed*³⁹,
*S. Reito*²¹, *L.K. Resvanis*^{4,41}, *G. Riccobene*²⁴, *R. Richter*¹², *K. Roensch*¹², *J. Rolin*¹⁷, *J. Rose*³⁶,
*J. Roux*⁹, *A. Rovelli*²⁴, *A. Russo*²⁷, *G.V. Russo*²², *F. Salesa*¹⁶, *D. Samtleben*³⁹, *P. Sapienza*²⁴,
*J.-W. Schmelling*³⁹, *J. Schmid*¹², *J. Schnabel*¹², *K. Schroeder*⁸, *J.-P. Schuller*⁶, *F. Schussler*⁶,
*D. Sciliberto*²¹, *M. Sedita*²⁴, *T. Seitz*¹², *R. Shanidze*¹², *F. Simeone*³⁰, *I. Siotis*³⁸, *V. Sipala*²⁰,
*C. Sollima*²⁸, *S. Sparnocchia*⁸, *A. Spies*¹², *M. Spurio*¹⁹, *T. Staller*³⁴, *S. Stavrakakis*¹⁴,
*G. Stavropoulos*⁴¹, *J. Steijger*³⁹, *Th. Stolarczyk*⁶, *D. Stransky*¹², *M. Taiuti*²³, *A. Taylor*¹¹,
*L. Thompson*⁴², *P. Timmer*³⁹, *D. Tonoiu*³³, *S. Toscano*¹⁶, *C. Touramanis*³⁷, *L. Trasatti*²⁵,
*P. Traverso*⁸, *A. Trovato*²⁴, *A. Tsigotis*¹⁵, *S. Tzamarias*¹⁵, *E. Tzamariudaki*³⁸, *F. Urbano*¹⁶,
*B. Vallage*⁶, *V. Van Elewyck*³, *G. Vannoni*⁶, *M. Vecchi*⁹, *P. Vermin*⁶, *S. Viola*²⁴, *D. Vivolo*²⁷,
*S. Wagner*¹², *P. Werneke*³⁹, *R.J. White*³⁶, *G. Wijnker*³⁹, *J. Wilms*¹², *E. de Wolf*^{2,39}, *H. Yepes*¹⁶,
*V. Zhukov*⁴¹, *E. Zonca*⁶, *J.D. Zornoza*¹⁶, and *J. Zúñiga*¹⁶

- ¹ *University of Aberdeen, United Kingdom*
- ² *University of Amsterdam, the Netherlands*
- ³ *APC – AstroParticule et Cosmologie – UMR 7164 (CNRS, Université Paris 7, CEA, Observatoire de Paris), Paris, France*
- ⁴ *University of Athens, Greece*
- ⁵ *University of Barcelona, Spain*
- ⁶ *CEA, IRFU, Centre de Saclay, 91191 Gif-sur-Yvette, France*
- ⁷ *CEA-CNRS-UVSQ, LSCE/IPSL, 91198 Gif-sur-Yvette, France*
- ⁸ *CNR-ISMAR, La Spezia, Trieste, Genova, Italy*
- ⁹ *CPPM, Aix-Marseille Université, CNRS/IN2P3, Marseille, France*
- ¹⁰ *University of Cyprus*
- ¹¹ *Dublin Institute for Advanced Studies (DIAS), Ireland*
- ¹² *Erlangen Centre for Astroparticle Physics (ECAP), University of Erlangen–Nuremberg, Germany*
- ¹³ *Groupe de Recherche en Physique des Hautes Energies (GRPHE)/EA3438/Université de Haute Alsace, Colmar, France*
- ¹⁴ *Hellenic Centre for Marine Research (HCMR), Greece*
- ¹⁵ *Hellenic Open University, Patras, Greece*
- ¹⁶ *IFIC – Instituto de Física Corpuscular, CSIC and Universitat de València, Spain*
- ¹⁷ *IFREMER, France*
- ¹⁸ *INFN Sezione di Bari and University of Bari, Italy*
- ¹⁹ *INFN Sezione di Bologna and University of Bologna, Italy*
- ²⁰ *INFN Sezione di Cagliari and University of Sassari, Italy*
- ²¹ *INFN Sezione di Catania, Italy*
- ²² *INFN Sezione di Catania and University of Catania, Italy*
- ²³ *INFN Sezione di Genova and University of Genova, Italy*
- ²⁴ *INFN Laboratori Nazionali del Sud, Catania, Italy*
- ²⁵ *INFN Laboratori Nazionali di Frascati, Italy*
- ²⁶ *INFN Sezione di Napoli, Italy*
- ²⁷ *INFN Sezione di Napoli and University of Napoli, Italy*
- ²⁸ *INFN Sezione di Pisa and University of Pisa, Italy*
- ²⁹ *INFN Sezione di Roma, Italy*
- ³⁰ *INFN Sezione di Roma and University of Roma 1 “La Sapienza”, Italy*
- ³¹ *Istituto Nazionale di Geofisica e Vulcanologia (INGV), Italy*
- ³² *University of Strasbourg and Institut Pluridisciplinaire Hubert Curien/IN2P3/CNRS, Strasbourg, France*
- ³³ *Institute of Space Science, Măgurele-Bucharest, Romania*
- ³⁴ *University of Kiel, Germany*
- ³⁵ *KVI, University of Groningen, the Netherlands*
- ³⁶ *University of Leeds, United Kingdom*
- ³⁷ *University of Liverpool, United Kingdom*
- ³⁸ *National Center of Scientific Research “Demokritos”, Athens, Greece*
- ³⁹ *Nikhef, Amsterdam, the Netherlands*
- ⁴⁰ *Koninklijk Nederlands Instituut voor Onderzoek der Zee (NIOZ), Texel, the Netherlands*
- ⁴¹ *NOA/NESTOR, Pylos, Greece*
- ⁴² *University of Sheffield, United Kingdom*
- ⁴³ *Tecnomare, Venice, Italy*
- ⁴⁴ *University of Utrecht, the Netherlands*
- ⁴⁵ *Institut d’Investigació per a la Gestió integrada de les Zones Costaneres, Universitat Politècnica València, Gandia, Spain*

^a also at *Université Paris-Sud, 91405 Orsay Cedex, France*

^b now at *Universität Würzburg, Germany*

^c on leave of absence at *Humboldt University, Berlin, Germany*

^d now at *Dept. of Physics and Wisconsin IceCube Particle Astrophysics Center, University of Wisconsin, Madison, WI 53706, USA*

^e also at *Moscow State University, Skobeltsyn Institute of Nuclear Physics, Moscow, Russia*

^f now at *Bogolyubov Institute for Theoretical Physics, Ukraine*

^g now at *Laboratoire d'Annecy-le-Vieux de physique des particules (LAPP), France*

^h now at *Institut for Cosmic Ray Research, University of Tokyo, Japan*

ⁱ now at *Université Paris VI, Laboratoire de Physique Nucléaire et de Hautes Energies (LPNHE), France*

E-mail: o.kavatsyuk@rug.nl, loehner@kvi.nl

ABSTRACT: Detection of high-energy neutrinos from distant astrophysical sources will open a new window on the Universe. The detection principle exploits the measurement of Cherenkov light emitted by charged particles resulting from neutrino interactions in the matter containing the telescope. A novel multi-PMT digital optical module (DOM) was developed to contain 31 3-inch photomultiplier tubes (PMTs). In order to maximize the detector sensitivity, each PMT will be surrounded by an expansion cone which collects photons that would otherwise miss the photocathode. Results for various angles of incidence with respect to the PMT surface indicate an increase in collection efficiency by 30 % on average for angles up to 45° with respect to the perpendicular. Ray-tracing calculations could reproduce the measurements, allowing to estimate an increase in the overall photocathode sensitivity, integrated over all angles of incidence, by 27 % (for a single PMT). Prototype DOMs, being built by the KM3NeT consortium, will be equipped with these expansion cones.

KEYWORDS: Large detector systems for particle and astroparticle physics; Cherenkov detectors; Optical detector readout concepts; Instrument optimization.

*Corresponding author.

†Corresponding author.

Contents

1. Introduction	1
2. Multi-PMT DOM	2
3. The expansion cone: idea and implementation	3
4. Test bench	6
5. Results	8
6. Simulation	12
7. Summary and Discussion	14

1 Introduction

1 KM3NeT [1] is a future deep-sea research infrastructure hosting a neutrino telescope with a volume
2 of several cubic kilometers to be constructed in the Mediterranean Sea. The design, construction
3 and operation of the KM3NeT neutrino telescope will be pursued by a consortium formed by
4 numerous research institutes currently involved in the ANTARES [2], NEMO [3] and NESTOR [4]
5 pilot projects. These Mediterranean pilot projects have been exploring the technologies, building
6 prototypes and deploying small scale telescopes. Since May 30, 2008, the ANTARES underwater
7 neutrino telescope has been fully operational. Although being the largest neutrino detector viewing
8 the Galactic Center through the Earth as a shield against atmospheric muons, an efficient search for
9 high-energy (1-1000 TeV) neutrinos originating from galactic and extra-galactic sources requires a
10 much larger deep-sea Neutrino Telescope.
11

12 The detection principle exploits the measurement of Cherenkov light emitted by charged sec-
13 ondary particles resulting from neutrino interactions in the matter surrounding the telescope. Ac-
14 curate measurements of the light arrival times and amplitudes are required. These, together with a
15 precise knowledge in real time of the positions and orientations of the photosensors, are mandatory
16 to reconstruct the direction of the neutrinos with an angular resolution better than 0.3° for neutrino
17 energies above a few TeV. Such a precision on the measurement of the neutrino direction is a key
18 ingredient to reach the necessary sensitivity on point-like cosmic neutrino sources in a few years
19 of operation. In order to improve the rejection of environmental background and to increase the
20 sensitivity to high energy neutrinos, a digital optical module (DOM) with an arrangement of 31
21 3-inch photomultiplier tubes (PMTs) has been designed.

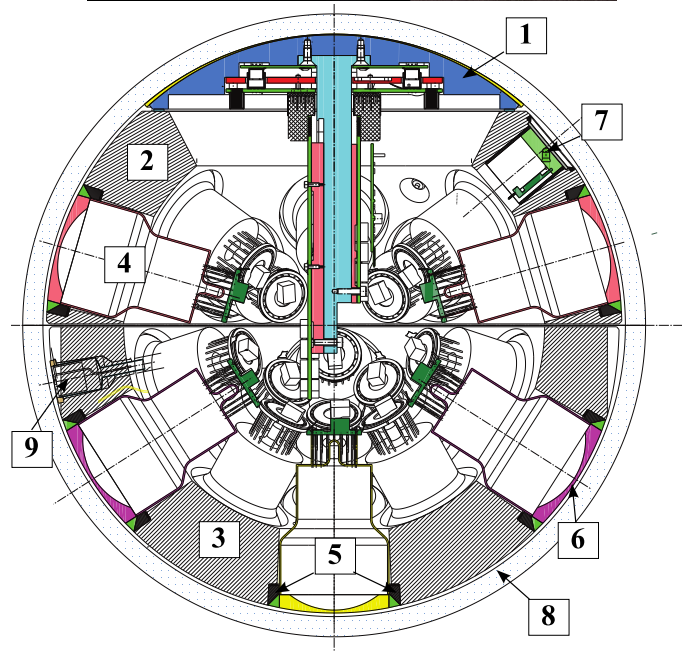


Figure 1. *Upper panel:* A mechanical reference model of a multi-PMT DOM with reflectors surrounding 3-inch PMTs. A single reflector is shown in the insert.

Lower panel: Cross section of a multi-PMT DOM [6] revealing the dense packing of readout electronics inside. Numbers refer to: 1-Heat conductor, 2,3-Foam cores, 4-PMT with PMT base, 5-Expansion cone, 6-Optical coupler, 7-Nanobeacon, 8-Glass sphere, 9-Piezo element.

22 **2. Multi-PMT DOM**

23 The multi-PMT DOM is an alternative to the conventional approach using one single 10-inch PMT
 24 or larger, and has several advantages. The total photocathode area that can be fitted in a standard
 25 17-inch diameter glass pressure sphere is significantly larger when using many small PMTs as com-
 26 pared to a single large PMT. The segmentation of the detection area in the multi-PMT DOM will
 27 aid in distinguishing single-photon from multi-photon hits. Two-photon hits can be unambiguously

28 recognized if the two photons hit separate tubes. Photons arriving in a plane wave from a particular
29 direction may be sensed by 7 PMTs on average. The probability that a signal corresponding to two
30 photo-electrons in a single 10-inch PMT is shared by two small PMTs is thus $(1 - 1/7) \approx 0.85$ [1].
31 Small PMTs can offer a quantum efficiency above 30%, provide a small transit time spread and do
32 not require shielding from the Earth's magnetic field. Also the reliability of the multi-PMT DOM
33 is higher since a failure of a single PMT will have much less impact on the performance of the
34 total DOM as compared to an optical module housing a single large PMT. Since handling the data
35 flow from the large number of PMTs in such a DOM becomes challenging, a cost-efficient readout
36 system is being developed [1, 5] with complete digitization inside the DOM.

37 The housing of the multi-PMT DOM (Fig. 1) is a transparent 17-inch glass sphere (VITRO-
38 VEX glass [7], wall thickness 14 mm), built to withstand the ambient hydrostatic pressure up to
39 600 bar. The sphere is separated into two hemispheres and contains the PMTs, the high-voltage
40 power supplies, front-end and readout electronics. The PMTs are suspended in a foam support
41 structure carrying 19 tubes in the lower and 12 in the upper hemisphere.

42 The center of the front face of each PMT is placed 4 mm from the inner surface of the glass
43 sphere. Optical gel fills the cavity between the foam support or the PMT front face and the glass
44 in order to assure optical contact (optical coupler). The foam support and the gel are sufficiently
45 flexible to allow for the deformation of the glass sphere under the hydrostatic pressure.

46 A mushroom-shaped aluminum structure transfers the heat generated by the DOM electronics
47 via the glass sphere to the seawater. For accurate muon reconstruction, it is necessary to know
48 the PMT positions with an accuracy of about 10 cm, and for this a position calibration system
49 is required. The multi-PMT DOM contains three calibration devices: the compass-tiltmeter, the
50 acoustic piezo sensor, and the nanobeacon, a compact low-cost nanosecond light flasher. More
51 details on the multi-PMT DOM can be found in Ref. [6, 8].

52 The dense packing constrains the space available for power supply and readout in the center
53 of the DOM. However, the optimal electro-optical design of the PMT leaves extra space between
54 neighboring PMTs on the inner surface of the sphere, surrounding the cathode entrance window
55 (see Fig. 1). To exploit this extra space for light collection, a reflector (expansion cone) will be
56 employed to guide additional light to the photocathode. The Photonis XP53B20 PMT, that passed
57 the specification requirements of KM3NeT except the dark-current performance, has a concave-
58 convex shaped glass window with a thickness of about 9 mm at the circumference and provides
59 a curved photocathode for optimum light collection and fast timing properties. PMTs with simi-
60 lar performance parameters are presently commercially available from several manufactures. The
61 thickness of the entrance window leaves space available for the entrance of light from the side onto
62 the curved photocathode. Results of tests will be presented for an expansion cone made of silicone
63 gel [9] which is shaped and kept in place by an aluminum structure serving as reflector, shown
64 schematically in Fig. 2. The reflectivity of the 45° tilted surface was improved by silver evapora-
65 tion. In order to demonstrate the potential benefit of the expansion cone, measurements in air and
66 with a single PMT have been performed.

67 **3. The expansion cone: idea and implementation**

68 Each PMT in the multi-PMT DOM will be surrounded by an expansion cone designed to collect

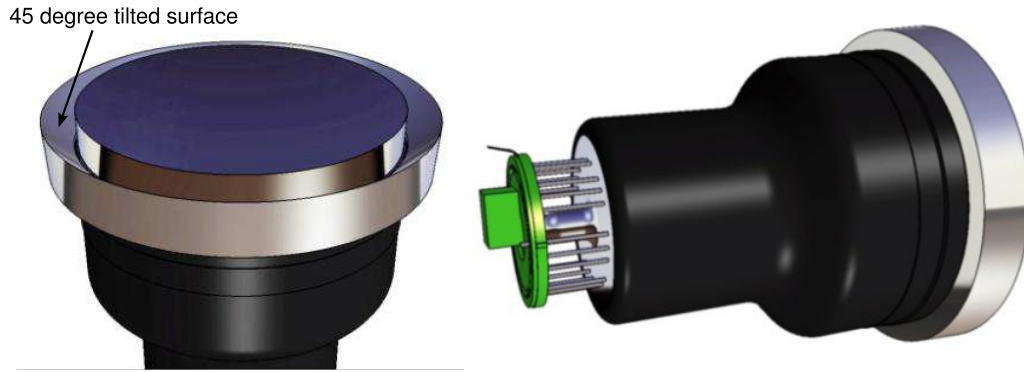


Figure 2. A drawing of the expansion cone mounted on a PMT.

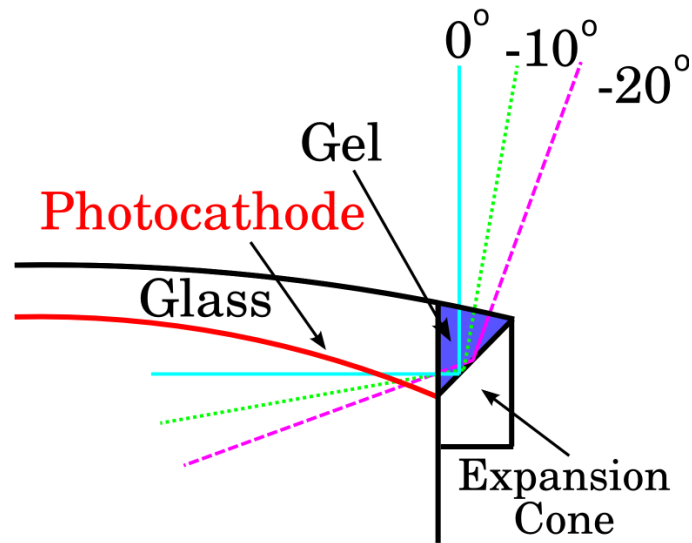


Figure 3. The idea of light collection by an expansion cone.

69 photons that would otherwise miss the photocathode, thus increasing the effective photocathode
 70 area (Fig. 1). The main idea behind such an expansion cone is demonstrated in Fig. 3. The light
 71 that comes aside of the PMT entrance window is reflected by the 45° tilted surface into the pho-
 72 tocathode. Ray-tracing simulations were performed for various opening angles of the expansion
 73 cone. The opening angle of 45° is optimized for maximum collection of light coming perpendicular
 74 to the PMT entrance window, which is essential for the direction reconstruction. The silicone gel
 75 serves as an optical interface, having a refractive index of 1.40 and the refractive index of the PMT
 76 entrance window is 1.54 (for photons of 420 nm wavelength).

77 For the performance tests, a 3-inch diameter Photonis XP53B20 PMT was used with main
 78 characteristics listed in Table 1. The Photonis XP53B20 tube has a compact Box & Linear struc-
 79 tured 10-stage electron multiplier allowing a short tube design required for a compact multi-PMT
 80 DOM. Moreover, it has a convex-shaped entrance window matched to the curvature of the glass
 81 sphere of the optical module (Fig. 1). In order to test the idea of such an expansion cone, measure-
 82 ments with a simplified setup were done. In comparison to the expansion cone to be used in the

Table 1. Characteristics of the used XP53B20 Photonis PMT from specifications and measurements.

	Photonis XP53B20
Window material	lime glass
Window curvature, R[mm]	198
Photocathode	improved Bi-alkali
QE [%]	33 (404 nm) [10]
Spectral range [nm]	290-700
Multiplier structure	10 stage
	Box & Linear
Time resolution, σ [ns]	2.30(0.02)*
Transit Time Spread [ns]	0.4*
Dark count rate [kHz]	5*

*detailed results and method described in [11]

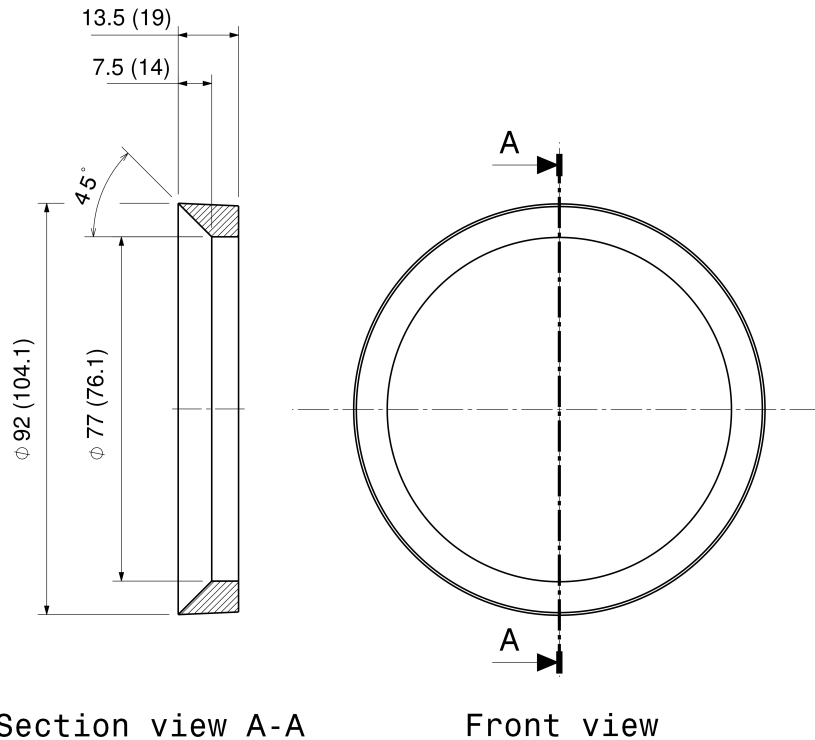


Figure 4. The expansion cone geometry to be used in the multi-PMT DOM. For the performance tests an expansion cone with sizes as given in brackets was manufactured (details in text).

83 multi-PMT DOM [6], a cone with a larger diameter of 104 mm instead of 92 mm was manufactured
 84 from aluminum (Fig. 4). This cone allows to fill silicon gel up to the level of 1 mm above the edge
 85 at the circumference of the PMT, as shown in Fig. 5, without using a glass sphere. Further, the
 86 larger cone allows to eliminate edge effects as they appear in the test setup due to the finite size of
 87 the test beam.

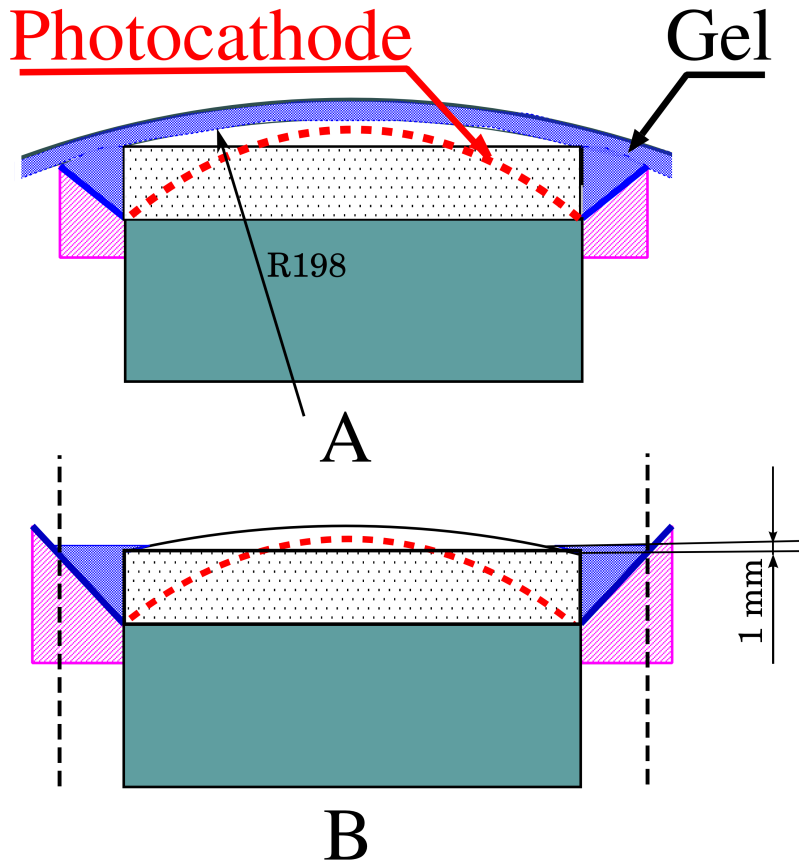


Figure 5. Silicon gel filled in the: *A.* Expansion cone geometry used in the multi-PMT DOM; *B.* Geometry used for tests. Silicone gel filled 1 mm above the edge at the circumference of the PMT. For the analysis, only data points limited to a radius $X < 46$ mm (dotted lines) were considered.

88 4. Test bench

89 The performance of the expansion cone was measured using a PMT socket with a built-in pre-
 90 amplifier (pre-amplification factor 62) in order to reduce heat dissipation, electronic noise and dark
 91 current. It allowed the operation at a PMT gain 1.2×10^6 with a high voltage of 950 V.

92 A PMT with the mounted expansion cone was placed inside a light-tight box (DarkBox). As a
 93 pulsed light source a laser¹ with wavelength $\lambda = 405$ nm and time jitter of < 70 ps between trigger
 94 and pulse was used. Additionally, a variable neutral density filter allowed to reduce intensities down
 95 to the level of single photo-electrons per pulse. A trigger output from the laser controller was used
 96 as a start signal for the data acquisition. The light from the laser was guided with a light fiber (core
 97 diameter 0.6 mm) inside the DarkBox and shone perpendicularly to the entrance window. This
 98 setup allowed a spot size of FWHM=1.4 mm at the center of the entrance window with a distance
 99 of 3 mm from the fiber to the PMT. Signal shapes were recorded by a fast sampling ADC². A
 100 remote-controlled 2D scanning system placed inside the DarkBox allowed precise measurements

¹Hamamatsu PLP10-40 laser diode head (wavelength 405 nm) with C10196 Controller.

²Acqiris DC282 digitizer with 10 bit resolution and 8 GS/s sampling rate.

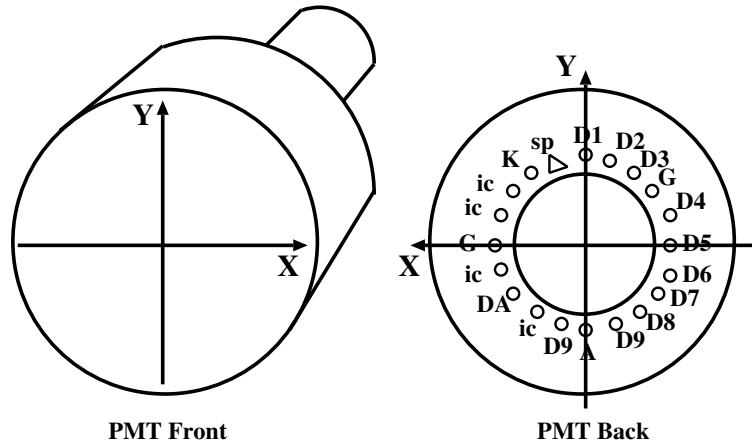


Figure 6. Coordinate system with origin at the center of the PMT entrance window used for the photocathode scan. The correspondence between the inner configuration of the electron multiplier and the pin-layout was used.

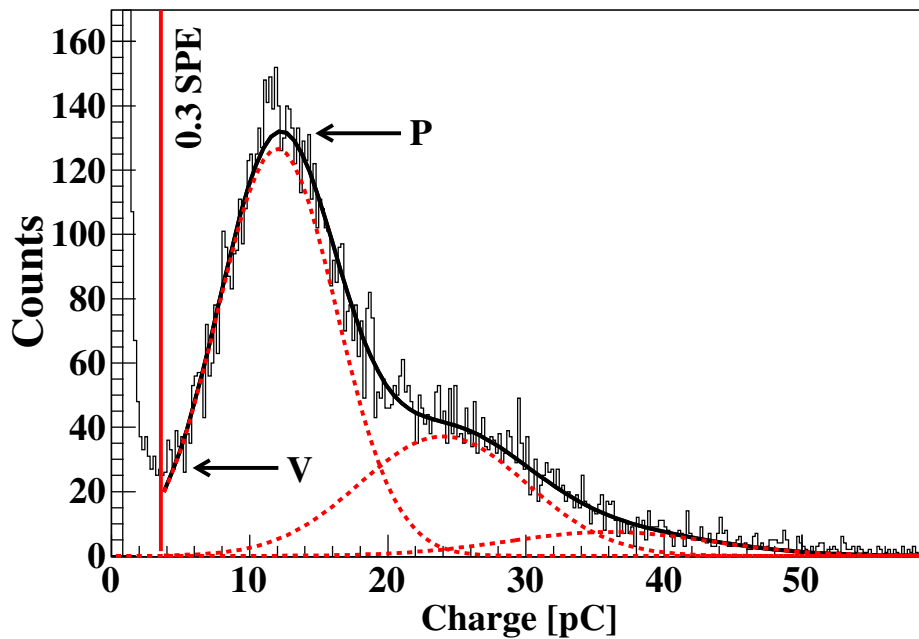


Figure 7. Typical measured charge distribution. PMT gain 1.2×10^6 , pre-amplification 62. The position of the peak (P) and valley (V) are indicated.

101 of the photocathode homogeneity and sensitivity with respect to position and angle of incidence.
 102 The scanning system consisted of two linear stages that allowed scanning in horizontal and vertical
 103 directions, equipped with stepper motors providing a repeatability of $1.5 \mu\text{m}$. The orientation of
 104 a PMT in the setup was defined by the orientation of the dynode structure. The origin of the
 105 coordinate system was the center of the entrance window. The Y axis lies in the plane of symmetry
 106 of the electron multiplier chain, perpendicularly to the dynodes. In practice, the correspondence
 107 between pin layout and inner configuration was used: the Y axis points from the anode to the first

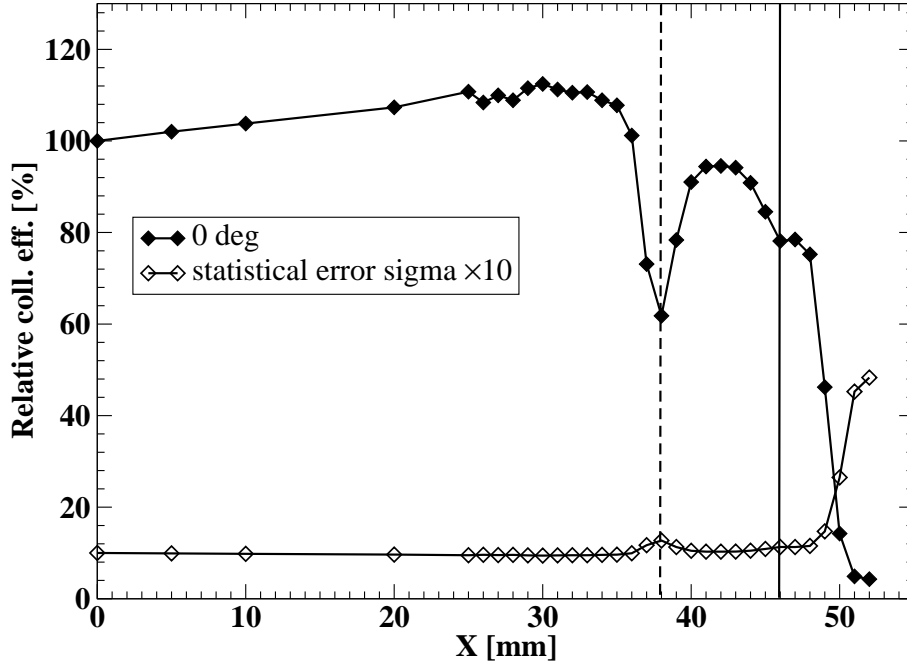


Figure 8. The relative collection efficiency for photon incidence perpendicular to the photocathode surface as a function of the radial position X on the photocathode, normalized to 100% at the center ($X=0$). Vertical lines indicate the position of the contact between the PMT and the expansion cone (dashed line), and the size of the expansion cone used in the multi-PMT DOM (solid line), respectively.

108 dynode pin (Fig. 6).

109 5. Results

110 A typical measured charge spectrum for a single point on the photocathode (center) is shown in
 111 Fig. 7. The position of the single-photoelectron (SPE) peak was determined and the PMT gain
 112 was derived. In Fig. 7 the contributions of one-, two- and three-PEs are separated by applying a
 113 deconvolution procedure according to [12]. The operation of a tube at a gain of 1.2×10^6 provides a
 114 good peak-to-valley ratio of about five. In order to determine the relative collection efficiency, the
 115 fraction of events with a charge above 0.3 SPE out of a total number of 20,000 accepted triggers
 116 was obtained for various points on the photocathode. The number of selected events for the center
 117 of the PMT was about 10,000.

118 In this work we compare the number of measured photon pulses for various positions on the
 119 photocathode and for a number of angles of incidence. The number of counts N_d is defined as
 120 $N_d = PDE \cdot N_p = QE \cdot CE \cdot N_p$, where PDE is the photon detection efficiency, N_p the number of
 121 incident photons, QE the quantum efficiency and CE the collection efficiency. We use the ratio
 122 $N_d(X)/N_d(0)$, where $N_d(0)$ is the number of counts collected in the centre of the photocathode,
 123 and $N_d(X)$ at any other point X . In the ratio, QE and N_p drop out (since we measure under the same
 124 conditions), resulting in the ratio of collection efficiencies $CE(X)/CE(0)$ or the relative collection
 125 efficiency. We assumed the collection efficiency in the centre of the entrance window (photocath-

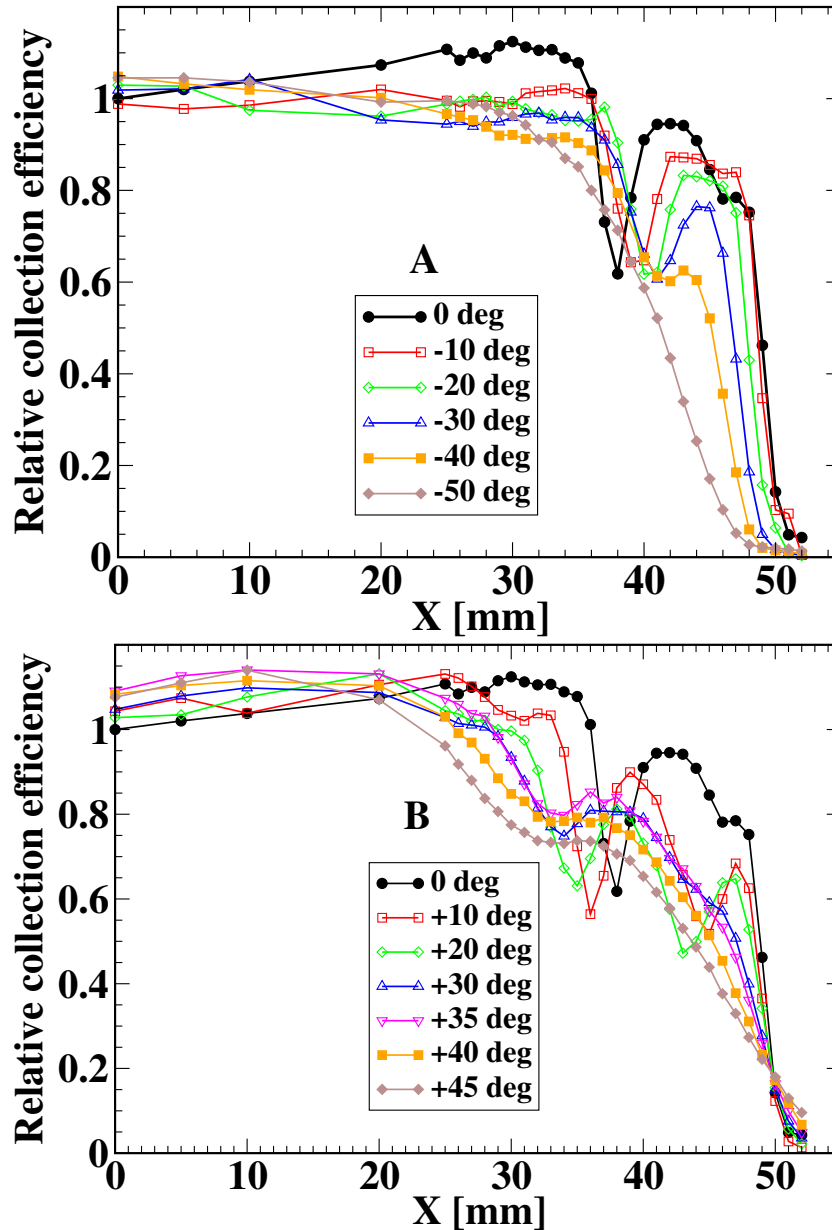


Figure 9. Measured relative collection efficiency as a function of the radial position X for various angles of incidence (see Fig. 3); *Upper panel:* for negative angles of incidence; *Lower panel:* for positive angles of incidence.

126 ode) to be 100% (for perpendicular incidence) and investigated the difference for the other points
 127 distributed on the photocathode and for various angles of incidence.

128 The relative collection efficiency as a function of the position on the photocathode is shown
 129 in Fig. 8 for the perpendicular incidence (0°). This results were obtained for a scan across the
 130 photocathode along the X -axis, measured at a temperature of 21°C . A dip in the relative collection
 131 efficiency curve observed at about $X=38$ mm can be explained by the expected decrease in the
 132 reflection on the contact between the PMT and the expansion cone and the thickness of the glass

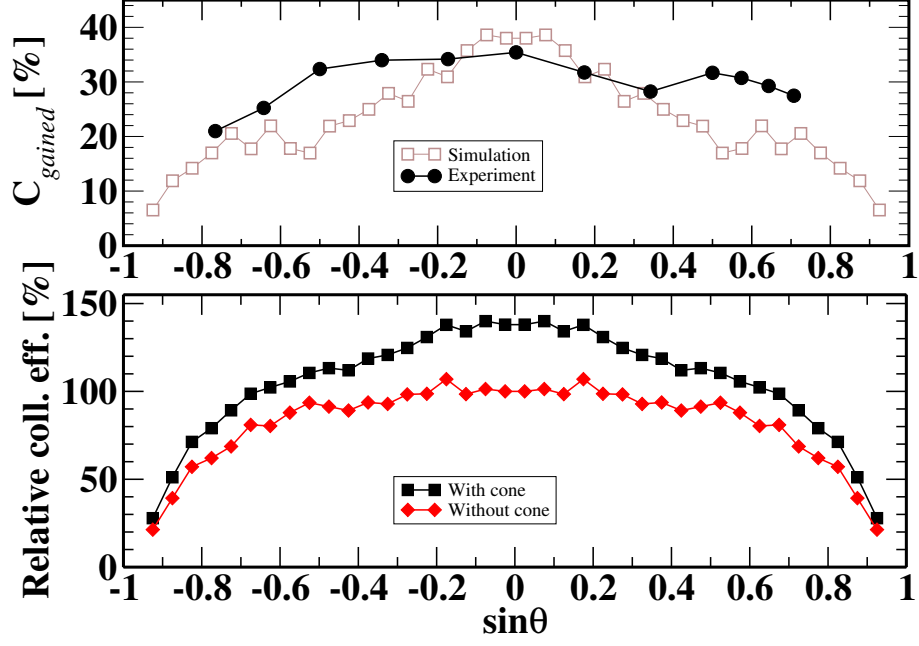


Figure 10. *Upper panel:* Gained collection efficiency along the X-axis according to Eq. 5.1, as a function of \sin of the angle of incidence θ . All presented data points have error bars of $C_{\text{gained}}[\%] \pm 0.04[\%]$. Results of the performed ray-tracing simulations are shown for comparison. *Lower panel:* Results of the ray-tracing simulations. Collection efficiency as a function of the angle of incidence for a single PMT with and without expansion cone (squares and diamonds, respectively).

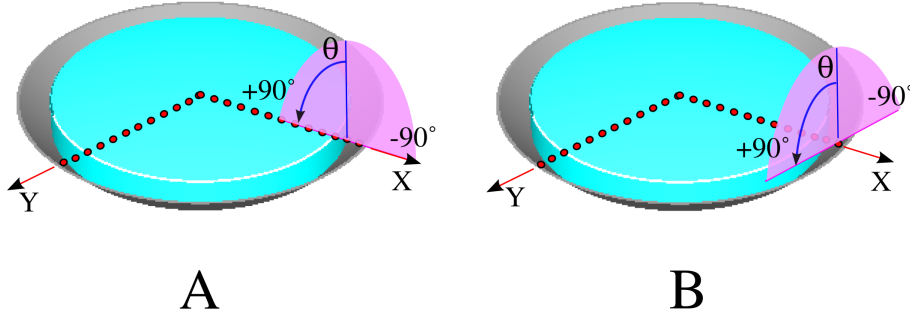


Figure 11. The expansion cone performance was tested with angles of incidence varied in two planes: parallel to the X-axis (A) and to the Y-axis (B).

133 wall. However, an additional experiment with a cone that could be moved axially has shown,
 134 that the observed decrease is not only caused by the effects mentioned above but also by the shift
 135 along the axial direction of the expansion cone relative to the photocathode. This assumption was
 136 confirmed by the performed ray-tracing simulations (see Section 6) and in previous extensive tests
 137 with an expansion cone made of PMMA [13]. The shoulder at 46-48 mm corresponds to the level
 138 to which the gel is filled (see Fig. 5).

139 Since every measured point X_v in the scan along the X direction represents an annulus with
 140 a width equal to the distance ΔX_v of neighboring measured points, weights $W(X_v)$ are applied

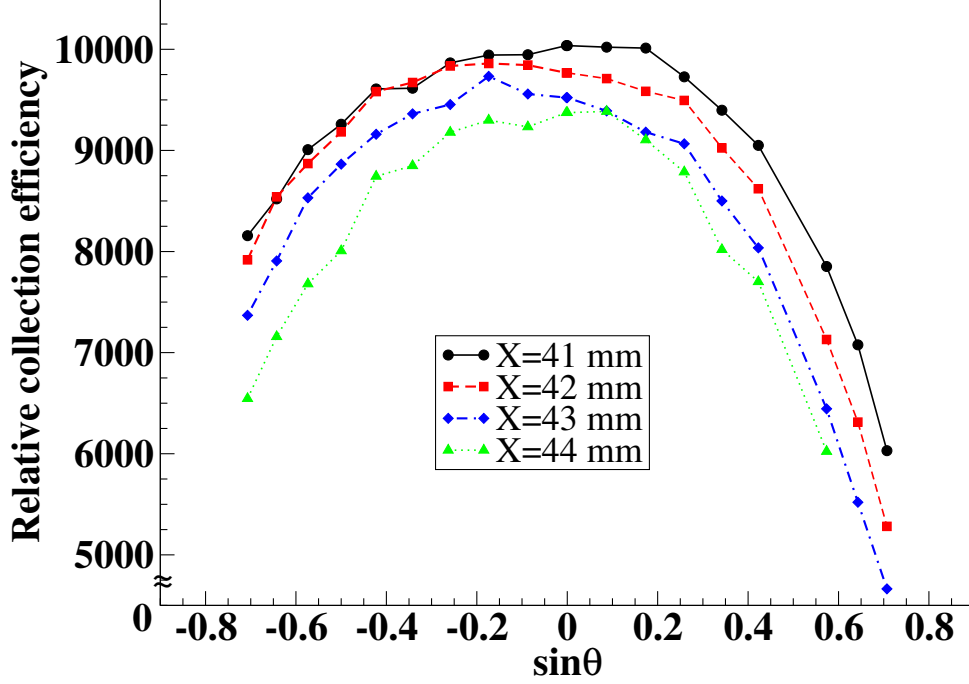


Figure 12. Measured relative light collection efficiency as a function of \sin of the angle of incidence θ in the plane parallel to the Y-axis (B in Fig. 11), for various radial positions on the expansion cone.

141 in order to account for the respective annular areas: $W(X_v) = \int_{\Delta X_v} 2\pi X dX$. The larger spacing
 142 between data points in the region $10 \text{ mm} < X < 25 \text{ mm}$ resulted in larger weighting factors for
 143 these points.

144 Results for the measurements with various angles of incidence are presented in Fig. 9. The def-
 145 inition of the sign of the angles of incidence is introduced in Fig. 3. In order to estimate the benefit
 146 of the expansion cone, the gained collection efficiency was calculated. For each angle of incidence
 147 the integral C_{PMT} was taken under the collection efficiency curve (Fig. 9) for the range (0 mm,
 148 38 mm), corresponding to the light entering directly in the photocathode. The integral $C_{PMT+Cone}$
 149 was taken for the range (0 mm, 46 mm) corresponding to the radial range of the expansion cone to
 150 be used in KM3NeT (Fig. 5). In Section 6 we demonstrate that the procedure of truncating a larger
 151 cone provides a realistic estimate of the light collection for the combination of PMT and expansion
 152 cone ($PMT + Cone$). Finally, the gained collection efficiency C_{gained} was estimated as a ratio

$$C_{gained} = \frac{C_{PMT+Cone} - C_{PMT}}{C_{PMT}} \times 100\%, \quad (5.1)$$

153 where $C_{PMT+Cone}$ and C_{PMT} are the collection efficiencies of the combination $PMT + Cone$ and
 154 PMT, respectively.

155 Results for the measurements under various angles of incidence are presented in Fig. 10, re-
 156 vealing an increase in collection efficiency by 30 % on average for angles of incidence from -50°
 157 to $+45^\circ$, with a maximum of 35 % for perpendicular incidence.

158 The results presented above were performed with angles of incidence varied in a plane parallel
 159 to the X-axis (A in Fig. 11), because of limitations of the scanning system. In order to account for

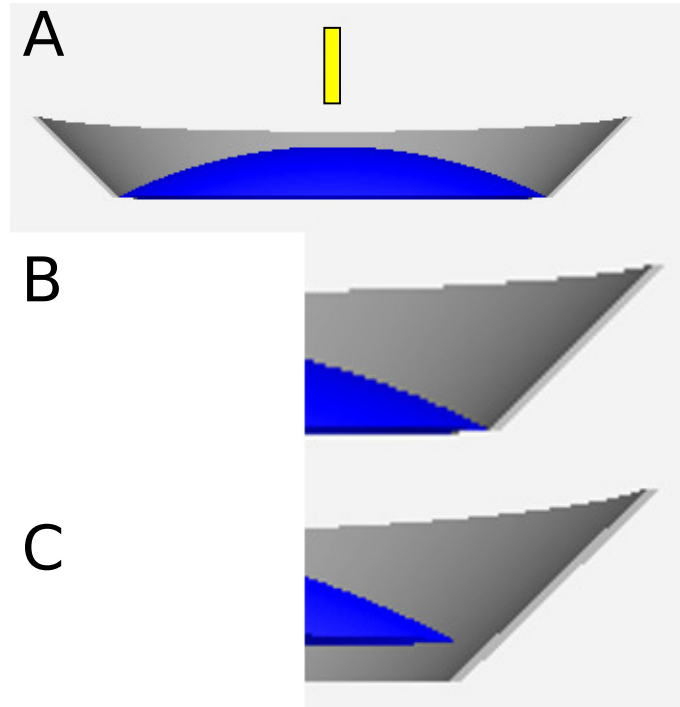


Figure 13. A. Simulated geometry (not to scale). The expansion cone is shown in gray, the photocathode in blue and the light guiding fiber in yellow on part A (used to reproduce the measured results). B. Zoomed view of the contact region between photocathode and expansion cone. C. Zoomed view of the geometry with an expansion cone that is slightly shifted axially relative to the photocathode (situation for the presented data).

160 effects for angles in the plane parallel to the Y-axis, measurements with configuration *B* (Fig. 11)
 161 were performed. Points with radius 41, 42, 43 and 44 mm were chosen to represent the performance
 162 of the expansion cone. Results presented in Fig. 12 follow a Gaussian-like distribution and agree
 163 well with distributions measured in the plane parallel to the X-axis (see Fig. 10 for comparison,
 164 configuration *A* in Fig. 11). The combined results allow to estimate the expansion cone performance
 165 rather well from data obtained for angles of incidence varied in one plane.

166 6. Simulation

167 Ray-tracing calculations were performed by using SLitrani [14], a general purpose Monte-Carlo
 168 program simulating light propagation. Even with a very simplified geometry (photocathode and
 169 aluminum expansion cone), shown in Fig. 13, the simulations reproduce the essential features of
 170 the distribution for the measured collection efficiency at perpendicular incidence (see Fig. 14 and
 171 8 for comparison). For this purpose a horizontal scan across the photocathode was simulated with
 172 light emitted perpendicularly from a light fiber producing a spot size of 1.4 mm FWHM on the
 173 photocathode. Results are shown in Fig. 14. In order to reproduce the experimental data points,
 174 a 1 mm axial shift of the expansion cone relative to the photocathode position was introduced.
 175 The obtained results, presented in Fig. 14, with different amplitudes in the contact region, confirm,

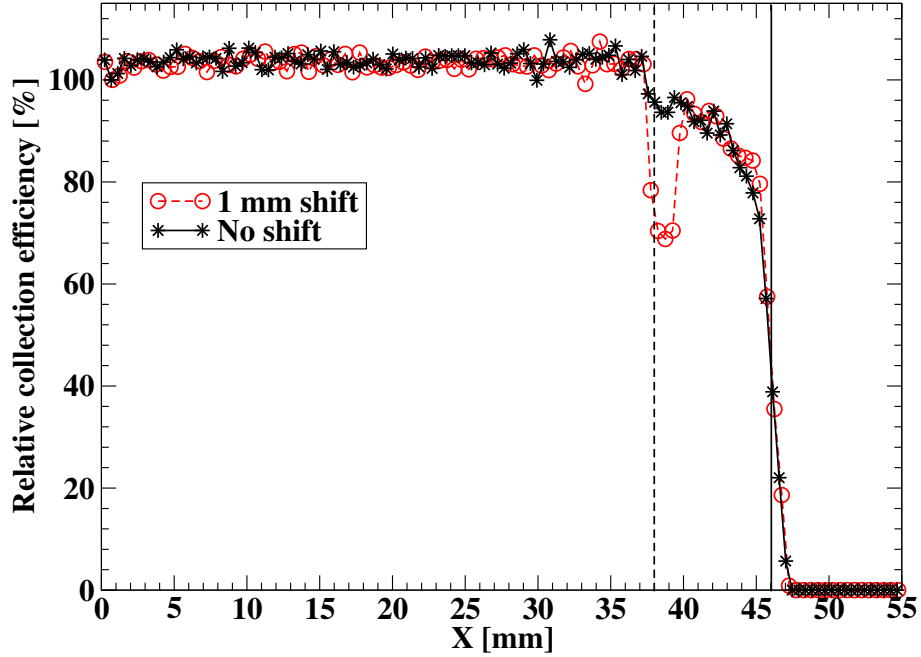


Figure 14. The relative collection efficiency obtained in the ray-tracing calculations with a pencil light beam. Stars correspond to the ideally aligned expansion cone of 46 mm radius. Circles show results obtained with an expansion cone of 46 mm radius that is shifted axially by 1 mm, reproducing well the essential features of the measured distribution presented in Fig. 8. Vertical lines indicate the position of the contact between the PMT and the expansion cone (dashed line), and the physical size of the expansion cone used in the multi-PMT DOM at 46 mm (solid line).

176 as discussed in Fig. 8, the shift in the axial position of the expansion cone. This underlines the
 177 importance to know the exact geometry of the photocathode.

178 In Section 5 the performance of the expansion cone in the multi-PMT DOM of KM3NeT was
 179 estimated by truncating experimental data measured for a 104 mm diameter cone. It should be
 180 noted that measurements were done with a light beam of 1.4 mm FWHM. The finite beam size
 181 creates edge effects because part of the beam will not be reflected when approaching the edge of
 182 the cone. This is demonstrated in Fig. 15 by comparing simulations for cone diameters of 104
 183 mm and 92 mm performed with light-beam diameters of 1.4 mm and 0.001 mm, respectively. The
 184 situation of the almost 0-size light beam corresponds to the situation of single photons hitting the
 185 cone in KM3NeT. This situation is very well reproduced by truncating data taken with a finite-size
 186 light beam and the larger cone at the radius of the cone which will be implemented in KM3NeT.

187 In order to estimate the collection efficiency integrated over all angles of incidence, a light
 188 emitting disk with 50 cm radius, much larger than the one of a PMT (3.8 cm) was simulated at a
 189 distance of 5 cm from the photocathode. In total 2×10^6 photons were emitted. The emission points
 190 were distributed uniformly over the light disk surface and the photon directions were uniformly
 191 distributed over the solid angle 2π . To compare to a configuration without an expansion cone, a
 192 photocathode was simulated together with a light absorbing foam core, to account for shadowing
 193 effects (see Section 2 and Fig. 1). These two simulated configurations are illustrated in Fig. 16.
 194 To assure that no light is reflected back to the cone or the photocathode, a totally absorbing plane

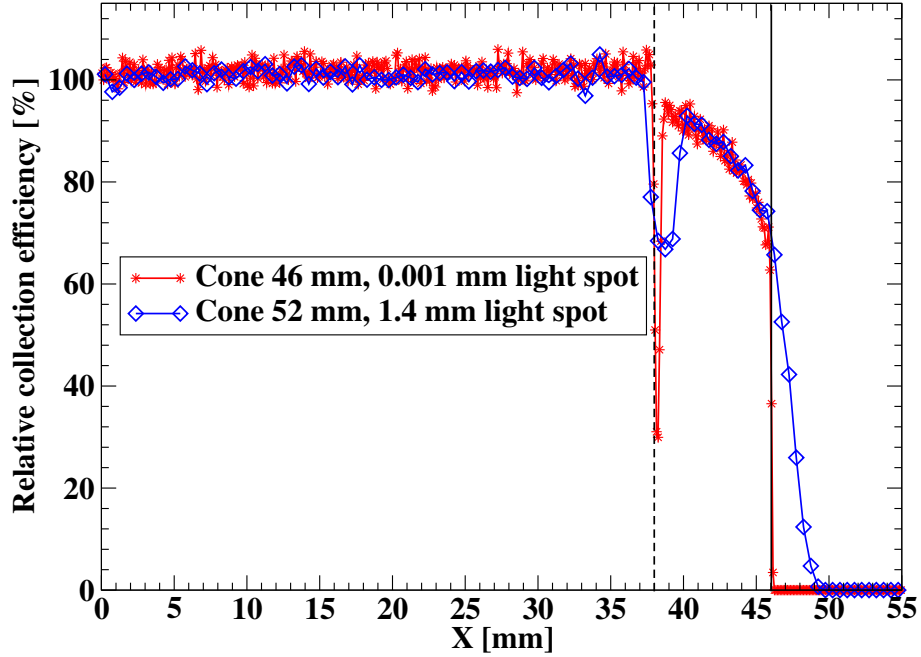


Figure 15. The relative collection efficiency obtained in the ray-tracing calculations with a pencil light beam. Stars show results obtained with an expansion cone of 46 mm radius and an almost 0-size light beam. Diamonds demonstrate results for an expansion cone of 52 mm radius as used in the measurements shown in Figs 8 and 9. Vertical lines indicate the position of the contact between the PMT and the expansion cone (dashed line), and the physical size of the expansion cone used in the multi-PMT DOM at 46 mm radius (solid line).

195 was included in the simulation. The simulation results reveal an increase in the overall sensitivity,
 196 integrated over all angles of incidence, by 27%.

197 The collection efficiency as a function of the angle of incidence was simulated. Results are
 198 presented in Fig. 10. The experimentally obtained curve for the gained collection efficiency (upper
 199 panel, Fig.10) is slightly asymmetric in comparison to the simulated one. The lower collection
 200 efficiency for $+10^\circ$ and $+20^\circ$ results from the curves shown in Fig. 9B, that exhibit a second dip at
 201 $X=45$ mm and $X=43$ mm, respectively. The cause for this phenomenon is schematically shown in
 202 Fig. 17, where light at certain angles can be reflected above the photocathode.

203 7. Summary and Discussion

204 In this work we demonstrated the performance of an expansion cone that is meant to enlarge the
 205 sensitive photocathode area of PMTs in a multi-PMT DOM for the future KM3NeT neutrino tele-
 206 scope. The expansion cone consisted of an aluminum ring filled with silicon gel and collects
 207 photons that would otherwise miss the photocathode. We have used a simplified experimental
 208 geometry to demonstrate the potential benefit of using such an expansion cone, and performed ex-
 209 tensive measurements on 3-inch PMTs with concave-convex shaped entrance window. This type of
 210 PMT is available for mass production and application in KM3NeT. Note, that the tested expansion
 211 cone was larger (exact sizes given in Fig. 4) in comparison to the one that will be used in the multi-

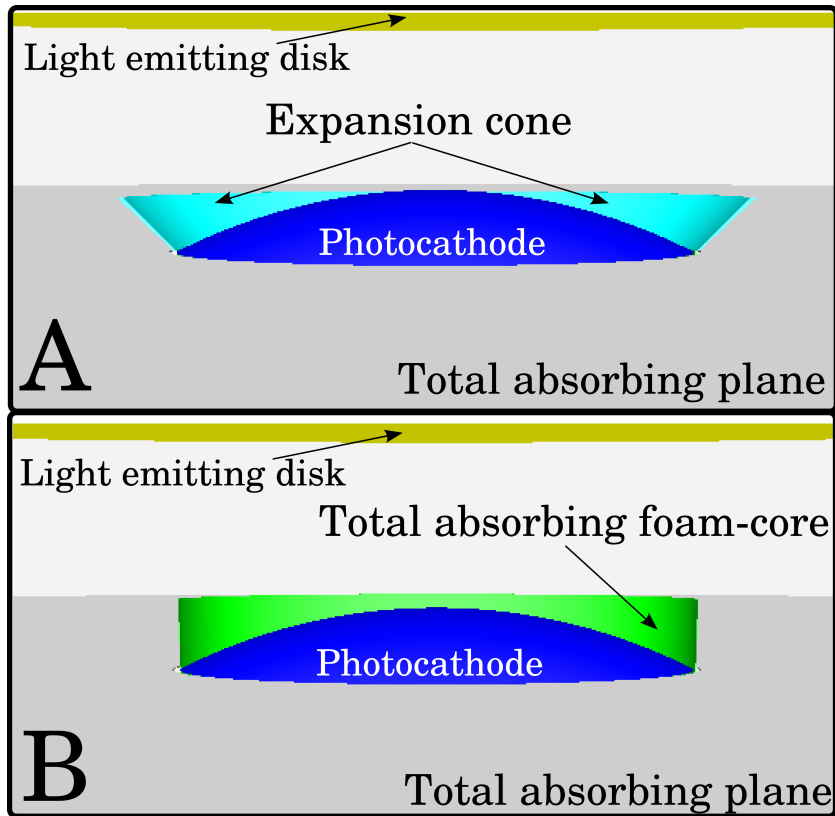


Figure 16. Simulated geometry with (A) and without (B) the expansion cone. The expansion cone, the photocathode, the light emitting disk, the totally absorbing plane, and the foam core are shown.

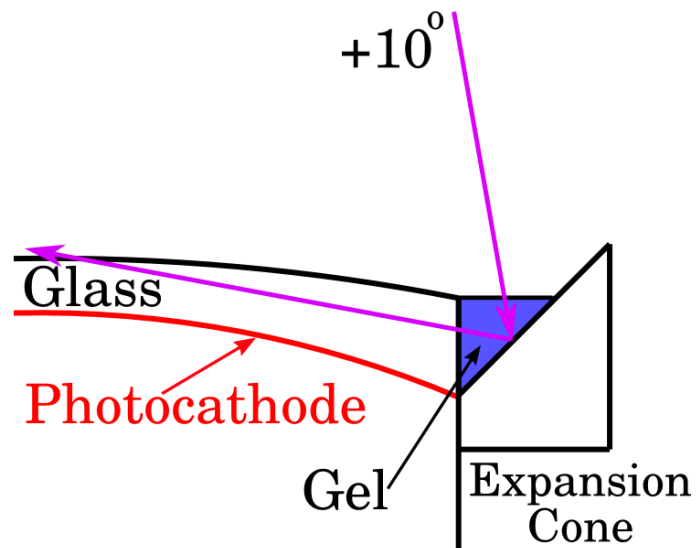


Figure 17. Schematic illustration of a light ray at an angle of incidence of $+10^\circ$, that can miss the photocathode due to reflection.

212 PMT DOM. However, due to the applied pencil light-beam scanning, it was possible to estimate
213 the realistic performance without edge effects for the expansion cone to be used in the multi-PMT
214 DOM by considering only data points limited to a radius $X < 46$ mm (Fig. 5).

215 Results for various angles of incidence indicate an increase in collection efficiency by 30 %
216 on average for angles of incidence from -50° to $+45^\circ$, with a maximum of 35 % for perpendicular
217 incidence. Ray-tracing simulations estimate an increase of the collection efficiency by 27% inte-
218 grated over all angles of incidence. Simulations and experiments have shown that the edges of the
219 photocathode are located higher than expected because of lacking information on the photocathode
220 geometry. This effect decreases the cone performance. In the future, precise information on the
221 photocathode geometry will be required from the producer. The proper alignment of the expan-
222 sion cone relative to the axial position of the photocathode is important to minimize the dip in the
223 collection efficiency at the contact between the expansion cone and the surface of the PMT.

224 A pencil light-beam has been applied in order to be able to scan precisely the collection ef-
225 ficiency at various locations on the surface of the photocathode. Alternatively, a light beam il-
226 luminating the whole PMT equipped with an expansion cone would be advantageous to estimate
227 the cone performance integrated over all angles of incidence. First tests with such a set-up were
228 reported in [15].

229 In order to obtain the final performance figures of the expansion cone in KM3NeT, measure-
230 ments under realistic conditions in sea water and with PMTs mounted in a glass sphere will soon
231 be possible using a DOM deployed in ANTARES.

232 Acknowledgments

233 This work is supported through the EU, FP6 Contract no. 011937, FP7 grant agreement no.
234 212252, and the Dutch Ministry of Education, Culture and Science.

236 References

- 237 [1] P. Bagley et al., KM3NeT Technical Design Report ISBN 978-90-6488-033-9,
238 <http://www.km3net.org/TDR/TDRKM3NeT.pdf>.
- 239 [2] M. Ageron et al., Nucl. Instrum. Meth. A 656 (2011) 11-38; arXiv:1104.1607v2.
- 240 [3] A. Capone et al., Nucl. Instrum. Meth. A 602 (2009) 47.
- 241 [4] P.A. Rapidis, Nucl. Instrum. Meth. A 602 (2009) 54.
- 242 [5] P. Kooijman, Nucl. Instrum. Meth. A 567 (2006) 508.
- 243 [6] Technical description of the PPM of the KM3NeT detection unit
244 http://www.km3net.org/PPM/KM3NeT_FL_REP_PPM-description.pdf.
- 245 [7] http://www.nautilus-gmbh.de/files/vitrovex_instrumentation_housings.pdf.
- 246 [8] O. Kavatsyuk, Q. Dorosti-Hasankiadeh, H. Löhner, Nucl. Instrum. Meth. A 695 (2012) 338.
- 247 [9] Wacker SilGel 612; <http://www.wacker.com>.
- 248 [10] B. Herold and O. Kalekin (2009), contribution to ICRC 2009;
249 <http://icrc2009.uni.lodz.pl/proc/pdf/icrc0596.pdf>.

- 250 [11] O. Kavatsyuk, Q. Dorosti-Hasankiadeh, H. Löhner, Nucl. Instrum. Meth. A 626-627 (2011) S154.
- 251 [12] E.H. Bellamy et al., Nucl. Instrum. Meth. A 339 (1994) 468.
- 252 [13] O. Kavatsyuk, Q. Dorosti-Hasankiadeh, G. Inguglia, and H. Löhner, contribution to ICRC 2009;
253 <http://icrc2009.uni.lodz.pl/proc/pdf/icrc0767.pdf>.
- 254 [14] F.X. Gentit, Nucl. Instrum. Meth. A 486 (2002) 35.
- 255 [15] O. Kalekin, J.J.M. Steijger, H.P. Peek, Nucl. Instrum. Meth. A 695 (2012) 313.